EnM
ENDOCRINOLOGY AND METABOLISM

Original Article

Endocrinol Metab 2022;37:290-302
https://doi.org/10.3803/EnM.2021.1343
pISSN 2093-596X · eISSN 2093-5978

Developmental Hypothyroidism Influences the Development of the Entorhinal-Dentate Gyrus Pathway of Rat Offspring

Ting Jin[1,2,*], Ranran Wang[1,3,*], Shiqiao Peng[1], Xin Liu[1], Hanyi Zhang[1], Xue He[1], Weiping Teng[1], Xiaochun Teng[1]

[1]Department of Endocrinology and Metabolism, Institute of Endocrinology, National Health Commission Key Laboratory of Thyroid Diseases, The First Affiliated Hospital of China Medical University, Shenyang; [2]Department of Endocrinology, Sir Run Run Shaw Hospital, Zhejiang University School of Medicine, Hangzhou; [3]Department of Endocrinology, Chifeng College Affiliated Hospital, Chifeng, China

Background: Developmental hypothyroidism impairs learning and memory in offspring, which depend on extensive neuronal circuits in the entorhinal cortex, together with the hippocampus and neocortex. The entorhinal-dentate gyrus pathway is the main entrance of memory circuits. We investigated whether developmental hypothyroidism impaired the morphological development of the entorhinal-dentate gyrus pathway.

Methods: We examined the structure and function of the entorhinal-dentate gyrus pathway in response to developmental hypothyroidism induced using 2-mercapto-1-methylimidazole.

Results: 1,1′-Dioctadecyl-3,3,3′,3′-tetramethylindocarbocyanine perchlorate tract tracing indicated that entorhinal axons showed delayed growth in reaching the outer molecular layer of the dentate gyrus at postnatal days 2 and 4 in hypothyroid conditions. The proportion of fibers in the outer molecular layer was significantly smaller in the hypothyroid group than in the euthyroid group at postnatal day 4. At postnatal day 10, the pathway showed a layer-specific distribution in the outer molecular layer, similar to the euthyroid group. However, the projected area of entorhinal axons was smaller in the hypothyroid group than in the euthyroid group. An electrophysiological examination showed that hypothyroidism impaired the long-term potentiation of the perforant and the cornu ammonis 3–cornu ammonis 1 pathways. Many repulsive axon guidance molecules were involved in the formation of the entorhinal-dentate gyrus pathway. The hypothyroid group had higher levels of erythropoietin-producing hepatocyte ligand A3 and semaphorin 3A than the euthyroid group.

Conclusion: We demonstrated that developmental hypothyroidism might influence the development of the entorhinal-dentate gyrus pathway, contributing to impaired long-term potentiation. These findings improve our understanding of neural mechanisms for memory function.

Keywords: Hypothyroidism; Neural pathways; Neuronal tract-tracers; Synaptic potentials; Axon guidance

Received: 27 November 2021, **Revised:** 21 January 2022, **Accepted:** 10 February 2022

Corresponding author: Xiaochun Teng
Department of Endocrinology and Metabolism, Institute of Endocrinology, National Health Commission Key Laboratory of Thyroid Diseases, The First Affiliated Hospital of China Medical University, No.155 Nanjing North Street, Shenyang 110001, China
Tel: +86-24-83282152, **Fax:** +86-24-83283294, **E-mail:** tengxiaochun@126.com

*These authors contributed equally to this work.

INTRODUCTION

In the past few decades, the developmental thyroid hormones, thyroxine and triiodothyronine, have been recognized as essential for neurodevelopment. A multi-center cohort study carried out by our group reported that hypothyroidism occurred in approximately 7.5% of pregnant women in China [1]. According to large population studies, the consequences of maternal hypothyroidism on offspring include low birth weight, a high rate of preterm birth, pregnancy loss, and impaired neurocognitive development (such as learning and memory) [2]. During normal neurological development, thyroid hormones act on the processes of neuronal proliferation and differentiation, cell migration, formation of layers, axonal and dendritic growth, synapse formation, and myelination [3,4].

Memory is stored in networks of brain neurons and through activity-dependent changes in the strength of synapses, according to Hebb's postulate. Long-term potentiation (LTP) is a relatively long-lived increase in the synaptic strength of fiber pathways. Giese et al. [5] generated a knock-in mouse model that lacked LTP, whose memory was thus strongly impaired. Moreover, researchers have observed LTP during learning, such as fear conditioning and one-trial inhibitory avoidance learning [6,7]. Furthermore, studies of cellular and molecular mechanisms have revealed extensive links between LTP and memory [8-10]. Many investigators now regard LTP as the neurophysiological model for learning and memory processes.

Animal studies have revealed that the hippocampus of offspring is particularly vulnerable to thyroid hormone deficiency during development, which contributes to learning and memory impairment [11-13]. Our research group has previously reported that maternal thyroid hormone deficiency led to LTP damage of the cornu ammonis 3 (CA3)-CA1 pathway in rat pups [14]. Gilbert and Paczkowski [15] also reported that LTP was impaired, as shown by reductions in the field excitatory postsynaptic potentials (fEPSP) slope, in the perforant pathway in pups treated with propylthiouracil, which depleted thyroid hormone by blocking hormone synthesis. Further research revealed dose-dependent impairment of LTP in the perforant pathway following maternal thyroid hormone insufficiency [11].

Memory function depends on the extensive neuronal circuits of the entorhinal cortex, together with the hippocampus and neocortex [16,17]. Information flow through the neuronal circuits contributes to hippocampal-dependent memory. The entorhinal-hippocampal circuit has been recognized as the classical memory circuit, being important for the formation and retrieval of declarative memories [18]. The granule cells of the dentate gyrus receive projections from the entorhinal cortex via the perforant pathway and send fibers to the CA3 region. CA3 neurons project Schaffer collaterals to the CA1 neurons (Fig. 1A) [19,20]. The dentate gyrus acts as the main entrance of the hippocampus, where the transmission of entorhinal information occurs [21]. Meanwhile, the dentate gyrus is involved in spatial pattern separation, and the CA1 and CA3 regions are involved in temporal pattern separation. This pattern separation has been suggested to decrease the

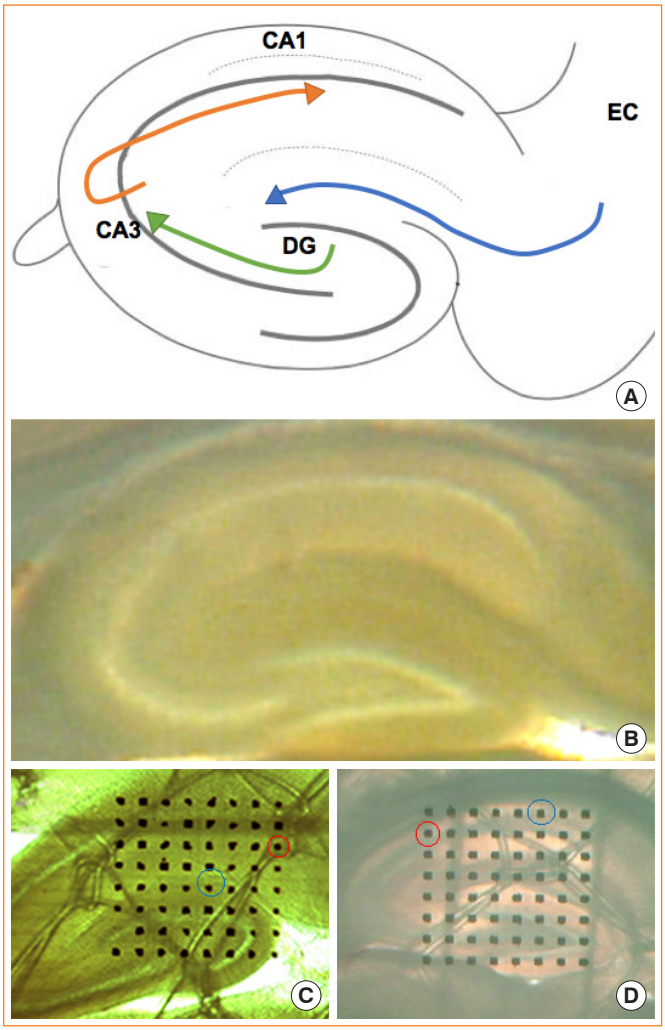

Fig. 1. Representative images of the entorhinal-hippocampal pathway. (A) Schematic drawing of the development of the entorhinal-hippocampal pathway. (B) Brain slices containing the maximum cross-sectional areas of the hippocampus were chosen for the electrophysiological experiments. (C, D) Microelectrode array covering the perforant pathway (C) or CA3-CA1 pathway (D). One microelectrode was selected as the stimulation site (red circle), which can induce the best synaptic responses in the recording site (green circle). CA, cornu ammonis; DG, dentate gyrus; EC, entorhinal cortex.

similarity among short-term memory representations and enhance the uniqueness of each representation, which is crucial for the hippocampus to establish long-term memory [22].

Thyroid hormone deficiency has deleterious effects on the development of hippocampal structures, such as a reduction in neuron number, impaired growth of axons, impaired dendritic arborization, and disrupted cell migration [23-25]. Hypothyroidism also influences the expression of various growth factors that are important to the regulation of axon elongation and guidance in the hippocampus [26,27]. The above-mentioned mechanisms and regulations are indispensable for the correct construction of neuronal circuits. Pathfinding by developing entorhinal axons towards the dentate gyrus is an essential step in establishing the entorhinal-dentate gyrus pathway. Several axon guidance molecules participate in pathfinding development, including attractive and repulsive axon guidance molecules. Both the perforant pathway and the CA3-CA1 pathway belong to the entorhinal-hippocampal circuit. The entorhinal-dentate gyrus pathway acts as the main entrance of entorhino hippocampal circuits. We speculated that the action of thyroid hormones on the morphological development of the entorhinal-dentate gyrus pathway would contribute to LTP alterations that ultimately lead to learning and memory impairment.

METHODS

Animals and treatments

Sixty nulliparous female Wistar rats weighing 180 to 200 g were housed in a temperature-controlled animal facility with a reversed 12:12-hour light/dark cycle. All rats were fed normal rat chow. All animals and experimental procedures were approved by the Animal Care and Use Committee at the China Medical University (Permit#: TZ2020009), which complies with the National Institute of Health Guide for the Care and Use of Laboratory Animals. The day of visualization of spermatozoa in vaginal smears was taken as embryonic (E) day 0. The day of birth was designated as postnatal (P) day 0. The pregnant rats were divided randomly into euthyroid (n=30 dams) and hypothyroid (n=30 dams) groups. To induce developmental hypothyroidism, a thyrotoxicant (2-mercapto-1-methylimidazole [MMI]; 0.025% w/v; 301507, Sigma, St. Louis, MO, USA), was given to pregnant rats in their drinking water from E6 and continued until the rats were sacrificed.

Assays for serum thyroid hormones

Dams were euthanized using sodium pentobarbital (50 mg/kg, delivered intraperitoneally) at four time points (E17, P2, P4, and P10), and blood samples were obtained by cardiac puncture. Pups were euthanized (sodium pentobarbital, 20 mg/kg, delivered intraperitoneally) and decapitated at P10, and trunk blood was collected. Blood samples were stored at –80°C and used to measure thyroid hormone levels. Total thyroxine (TT_4), total triiodothyronine (TT_3), and thyroid-stimulating hormone (TSH) levels were measured using chemiluminescence (Immulite 1000, Diagnostic Products Corporation, Los Angeles, CA, USA). The intra- and inter-assay coefficients of variation for TSH were 1.23%–3.38% and 1.57%–4.93%, respectively; for TT_4, they were 1.26%–3.20% and 3.58%–6.67%, respectively; and for TT_3, they were 1.31%–3.34% and 3.63%–5.57%, respectively.

Tract tracing

Pups at P2, P4, and P10 were euthanized (sodium pentobarbital, 20 mg/kg, delivered intraperitoneally) and their whole brains were fixed in 4% paraformaldehyde in 0.1 mmol/L phosphate-buffered saline (PBS, pH 7.2) for 1 to 2 days at room temperature. A lipophilic dye (1,1´-dioctadecyl-3,3,3´,3´-tetramethylindocarbocyanine perchlorate [DiI]; 468495; Sigma), was used to label the entorhinal-dentate gyrus pathway. Under a stereoscopic microscope (SZX7, OLYMPUS, Tokyo, Japan), signal crystals of DiI were injected into the entorhinal cortex using an acupuncture pin, as described previously [28]. The brain was stored in the dark at room temperature for 2 to 3 weeks. Thereafter, the brain was rinsed with PBS, embedded in 4% low-melting-point agarose, and sectioned horizontally using a vibratome (MA752, Campden Instruments, Loughborough, UK) at an 80-μm thickness. Sections were counterstained with Hoechst (B2883, Sigma) and observed with an epifluorescence microscope (BX-51, OLYMPUS). Image quantification analysis was performed using Image Pro Plus version 5.1 software (Media cybernetics, Rockville, MD, USA). The outer molecular layer of the dentate gyrus was outlined manually. At P2 and P4, the proportion of fibers in the outer molecular layer referred to the ratio of the area of DiI-labeled fibers to the total area of the outer molecular layer. At P10, the projected area in the outer molecular layer was represented by the DiI-labeled area. Each section was measured in triplicate.

LTP induction

Pups at P10 were euthanized by decapitation as described previously. The whole brain was rapidly dissected from the skulls and immersed in ice-cold oxygenated (95% oxygen and 5%

carbon dioxide mixed gas) artificial cerebrospinal fluid (ACSF) containing NaCl (7.25 g/L), KCl (0.22 g/L), $NaHCO_3$ (0.22 g/L), $MgSO_4$ (0.12 g/L), KH_2PO_4 (0.17 g/L), $CaCl_2$ (0.11 g/L), and dextrose (1.8 g/L), at a pH of 7.4 to 7.8. Then, the cerebellum, the frontal lobe, and the ventral-lateral areas (30° off the horizontal axis) were removed and perfused with 45°C low melting-temperature agarose. Brain slices (300 μm) containing the maximum cross-sectional areas of the hippocampus were cut using a vibratome (Fig. 1B) and incubated for 1 to 1.5 hours in ACSF at room temperature.

A 64-channel multi-electrode dish system (MED64, Panasonic Alpha-Med Sciences, Osaka, Japan) was used in this study. Procedures for the preparation of the multi-electrode dish probe were performed according to standard methods [29,30]. After incubation, the slice was positioned on the MED64 probe (an array of 64 square planar microelectrodes arranged in an 8×8 pattern) and most of the 64 microelectrodes were located within the hippocampus. According to photomicrographs of brain slices acquired under microscopy, one of the 64 available planar microelectrodes was selected to stimulate the perforant pathway (Fig. 1C) or the CA3-CA1 pathway (Fig. 1D). The evoked fEPSPs were amplified, digitized and recorded from the recording channels.

After selection of sites in the angular bundle or CA3 for stimulation, an input/output (I/O) curve was constructed from the fEPSP responses following a series of stimulations at ascending intensities (starting with 5 μA and increasing stepwise by 5 μA). A series of stimulations were delivered until the maximal fEPSP amplitude and slope were reached.

For the induction of LTP, the intensity of the test stimulus was determined using the I/O function and fixed at the intensity that produced 30% of the maximal fEPSP slope. A range of pulses was administered every 30 seconds for 10 minutes to record the baseline fEPSP. LTP was induced using high-frequency stimulation (HFS), consisting of a range of two pulses (at an interval of 2 seconds) at the pulse intensity that evoked 30% of the maximal fEPSP slope. The signal was recorded for 1 hour, and LTP values were expressed as percentages of the pre-stimulation baseline.

Quantitative real-time reverse transcription polymerase chain reaction analysis

At P2, P4, and P10, neonatal brains were perfused with physiological saline through the left ventricle and then removed. The hippocampi were dissected on ice and stored in liquid nitrogen. Total RNA was extracted from the hippocampi of pups from different litters using the Trizol reagent (15596026, Invitrogen, Waltham, MA, USA). RNA was reverse-transcribed into cDNA using a PrimeScript RT reagent kit (RR036A, Takara, Shiga, Japan). Transcripts were quantified using a SYBR Premix Ex Taq II kit (RR420A, Takara) according to the manufacturer's instructions. Polymerase chain reaction (PCR) was performed in a total volume of 20 μL using a LightCycler 480 Instrument (Roche Applied Science, Mannheim, Germany). The primers for the selected genes used in real-time PCR are listed in Supplemental Table S1, including *Ntn1* (encoding netrin 1 [Ntn1]), *Efna3* (encoding erythropoietin-producing hepatocyte ligand A3, also known as ephrin A3 [Efna3]), *Sema3a* (encoding semaphorin 3A [Sema3a]), and *Rgma* (encoding repulsive guidance molecule BMP co-receptor A [Rgma]).

Western blotting

The hippocampi of pups were dissected and collected at P2, P4, and P10. The tissues were homogenized in 100 μL of lysis buffer containing 10 μL of phosphatase inhibitors and 1 μL of protease inhibitors. The homogenate was centrifuged at 10,000 ×*g* for 10 minutes at 4°C. The supernatant was taken for protein determination. The protein concentration was determined using a bicinchoninic acid assay. Protein (100 μg) was boiled for 3 minutes and separated on 10% sodium dodecyl sulfate-polyacrylamide gels followed by transfer onto polyvinylidene difluoride membranes. After blocking with PBS including 0.1% Tween-20 and bovine serum albumin for 1 hour at room temperature, the membrane was incubated overnight with primary antibodies recognizing ephrin A3 (1:1,000, ab64814, Abcam, Cambridge, UK) or semaphorin 3A (1:1,000, ab23393, Abcam). Subsequently, the membrane was incubated with horseradish peroxidase-conjugated secondary antibody (1:5,000, SAB370119, Sigma). Immune complexes were visualized using a chemiluminescence Western blotting detection system (ALPHAVIEW, Proteinsimple Inc., San Jose, CA, USA).

Statistical analyses

Data are presented as the mean±standard deviation. All analyses were performed using SPSS version 17.0 (SPSS Inc., Chicago, IL, USA). Data that conformed to a normal distribution were analyzed using the Student *t* test, and data that did not conform to a normal distribution were analyzed using the rank-sum test. In cases of heterogeneous variances, the Welch test was used. A $P<0.05$ was considered statistically significant.

RESULTS

Developmental hypothyroidism caused by MMI

After treatment with 0.025% MMI in drinking water from E6 onwards until the date of sacrifice (E17, P2, P4, and P10), the levels serum thyroid hormones (TT_3 and TT_4) of the dams decreased significantly at all time points ($P<0.001$). Meanwhile, the serum TSH level of the dams significantly increased compared with that in the euthyroid dams ($P<0.001$) (Table 1). During the early postnatal period (P10), the pups from MMI-treated pregnant rats demonstrated a significant increase in TSH and suppression of thyroid hormones (TT_3 and TT_4) compared with the levels in the control group ($P<0.001$) (Table 1). Thus, the animal model of developmental hypothyroidism was successfully established at the prenatal stage (E17). There were no significant differences in body weight between the groups of dams during the prenatal and postnatal stages (Table 2). Developmental exposure to MMI resulted in postnatal growth retardation of the pups. The mean body weight of the hypothyroid group pups was lower than that of the euthyroid group pups ($P<0.001$) (Table 3). The differences in postnatal weights between the two groups became larger with time, displaying a 28.2% reduction at P2, a 42.0% reduction at P4, and a 39.7% reduction at P10.

Developmental hypothyroidism impaired the development of the entorhinal-dentate gyrus pathway

To visualize the development of the entorhinal-dentate gyrus pathway under developmental hypothyroidism, we used DiI tract tracing to label fibers. At P2, the entorhinal fibers traversed into the angular bundle and branched into two main axonal projections. One ran superficially along the alveus (alvear path), and the other, the perforant pathway, was orientated in the stratum lacunosum moleculare of CA1. This phenomenon appeared in pups of both the euthyroid and hypothyroid groups (Fig. 2).

Implantation of DiI in the euthyroid pups yielded the typical layer-specific innervations of the entorhinal-dentate gyrus pathway. The DiI-labeled entorhinal axons innervated the stratum lacunosum moleculare, and at P2, a few axons started to cross the hippocampal fissure and distribute into the molecular layer of the dentate gyrus (Fig. 3A, arrows). From P4 onward, the fiber bundle that appeared in the molecular layer became distinct (Fig. 3C). At P10, the entorhinal-dentate gyrus projection displayed a layer-specific distribution in the outer molecular layer of the dentate gyrus (Fig. 3E).

Table 1. Serum Thyroid Hormone Levels in Dams and Pups

Animal	Stage	Euthyroid group			Hypothyroid group		
		TSH, mIU/L	TT_4, μg/dL	TT_3, ng/dL	TSH, mIU/L	TT_4, μg/dL	TT_3, ng/dL
Dams	E17	0.35±0.14	2.81±0.34	60.36±9.92	4.77±2.01[a]	1.15±0.31[a]	25.81±8.07[a]
	P2	0.20±0.12	2.40±0.73	68.28±11.92	8.97±2.49[a]	1.35±0.92[a]	18.56±3.42[a]
	P4	0.26±0.70	1.88±0.34	68.00±15.78	8.84±1.13[a]	1.09±0.30[a]	15.98±2.01[a]
	P10	0.45±0.07	1.66±0.40	53.26±1.72	11.77±1.78[a]	0.62±0.08[a]	12.36±3.62[a]
Pups	P10	0.23±0.17	2.28±0.50	28.66±6.83	5.15±2.25[a]	0.56±0.10[a]	11.96±2.62[a]

Values are expressed as mean±standard deviation ($n=5$ dams in each group; $n=10$ pups from 5 dams in each group).
TSH, thyroid-stimulating hormone; TT_4, total thyroxine; TT_3, total triiodothyronine; E, embryonic; P, postnatal day.
[a]$P<0.01$, compared with the euthyroid group.

Table 2. Prenatal and Postnatal Body Weight in Dams

Stage	Euthyroid group, g	Hypothyroid group, g
E17	324.72±18.17	331.78±10.77
P2	286.44±10.66	278.12±10.08
P4	284.32±12.77	279.76±5.96
P10	290.76±8.82	280.92±12.48

Values are expressed as mean±standard deviation ($n=5$ dams in each group).
E, embryonic day; P, postnatal day.

Table 3. Postnatal Body Weight in Pups

Stage	Euthyroid group, g	Hypothyroid group, g
P2	7.44±0.82	5.34±0.84[a]
P4	11.81±1.42	6.85±0.77[a]
P10	18.80±1.00	11.33±1.32[a]

Values are expressed as mean±standard deviation ($n=10$ pups from 5 dams in each group).
P, postnatal day.
[a]$P<0.01$, compared with the euthyroid group.

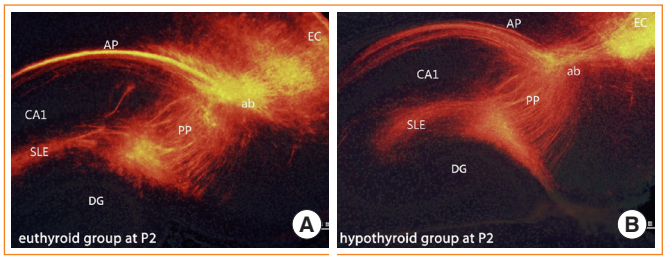

Fig. 2. Tracing the entorhinal-hippocampal pathway of (A) the euthyroid group and (B) the hypothyroid group at P2. DiI-labeled entorhinal fibers branched into the alvear path and the perforant pathway, which both appear in the euthyroid group and the hypothyroid group. Sections (n=10–12) were from different pups (n=4–6 pups from 4–6 dams) at P2. Scale bar, 200 μm. ab, angular bundle; AP, alvear path; CA, cornu ammonis; DG, dentate gyrus; EC, entorhinal cortex; PP, perforant pathway; SLE, stratum lacunosum moleculare; P, postnatal day.

In the pups of the hypothyroid group, entorhinal afferents ultimately reached their terminal field in the outer molecular layer. However, entorhinal axons showed delayed growth in reaching their appropriate target. At P2, few axons were distributed into the molecular layer (Fig. 3B). At P4, entorhinal axons were so sparse that no laminar distribution was identified in the molecular layer (Fig. 3D). The edge of entorhinal axons appeared to be further away from the granule layer than that of the euthyroid group. With further development (P10), the entorhinal-dentate gyrus pathway showed a layer-specific distribution in the outer molecular layer of the dentate gyrus, similar to the euthyroid group (Fig. 3F).

At P2, there was no statistically significant difference in the proportion of fibers in the outer molecular layer between the euthyroid and hypothyroid groups (Fig. 4A). This difference became prominent as fiber development proceeded. The proportion of fibers in the outer molecular layer of the hypothyroid group was significantly smaller than that of the euthyroid group (P<0.001) (Fig. 4B). We then studied the projected area into which the entorhinal fibers arrived in the outer molecular layer (Fig. 3E arrows). The DiI-labeled area was crescent-shaped, with an irregular boundary. The area in pups of the hypothyroid group was smaller than that of the euthyroid group (P=0.027) (Fig. 4C); however, there was no statistically significant difference in the maximum width of the projected area between the two groups.

Developmental hypothyroidism impaired LTP of the perforant pathway and CA3-CA1 pathway

After HFS was applied to the perforant pathway, LTP induction

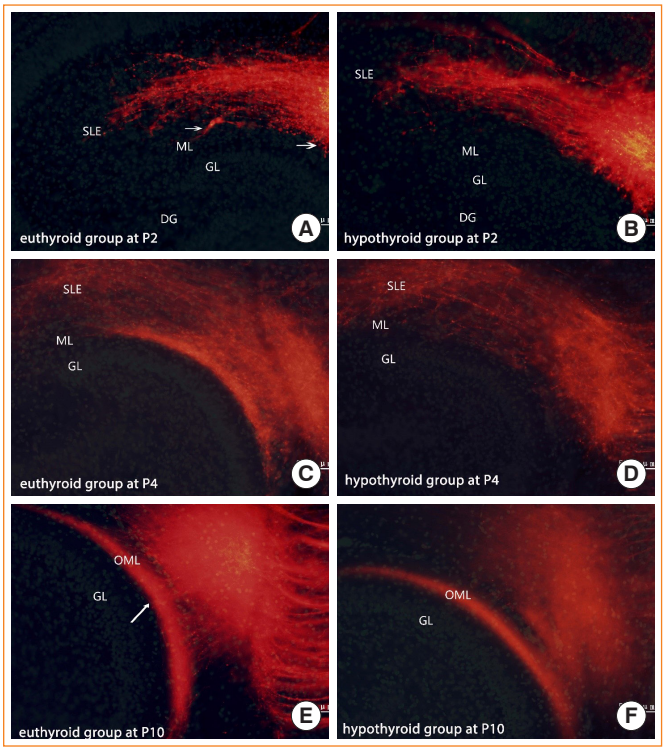

Fig. 3. Distribution of entorhinal axons in the dentate gyrus at (A, B) P2, (C, D) P4, and (E, F) P10. Photomicrographs of brain sections during the layer-specific distribution from (A, C, E) the euthyroid group and (B, D, F) the hypothyroid group. Euthyroid pup axons stared to distribute into the outer molecular layer (OML) at P2 (A, arrow), and displayed a layer-specific distribution in the OML at P10 (E, arrow). Hypothyroid pup axons reached the OML, as in euthyroid pups, but showed delayed development. Sections (n=10–12) were from different pups (n=4–6 pups from 4–6 dams) at P2, P4, and P10. Scale bar, 50 μm. DG, dentate gyrus; GL, granule layer; ML, molecular layer; SLE, stratum lacunosum moleculare; P, postnatal day.

was recorded. Both groups displayed increases in the fEPSP slope and amplitude (Fig. 5E, F). There was a non-significant difference in the fEPSP slope between the euthyroid slices and hypothyroid slices (euthyroid: 170.11%±43.55% of baseline; hypothyroid, 140.51%±19.80% of baseline, P=0.150) (Fig. 5A). However, the fEPSP amplitude of the hypothyroid slices was lower than that of the euthyroid slices (euthyroid: 160.77%±31.06% of baseline; hypothyroid: 133.29%±12.29% of baseline, P=0.036) (Fig. 5B).

Upon HFS, LTP was generated in the CA3-CA1 pathway from the euthyroid slices. In the hypothyroid group, both the fEPSP slope and the fEPSP amplitude were lower than those in the euthyroid group (fEPSP slope: 219.76%±69.30% of baseline in the euthyroid, 146.75%±32.65% of baseline in the hy-

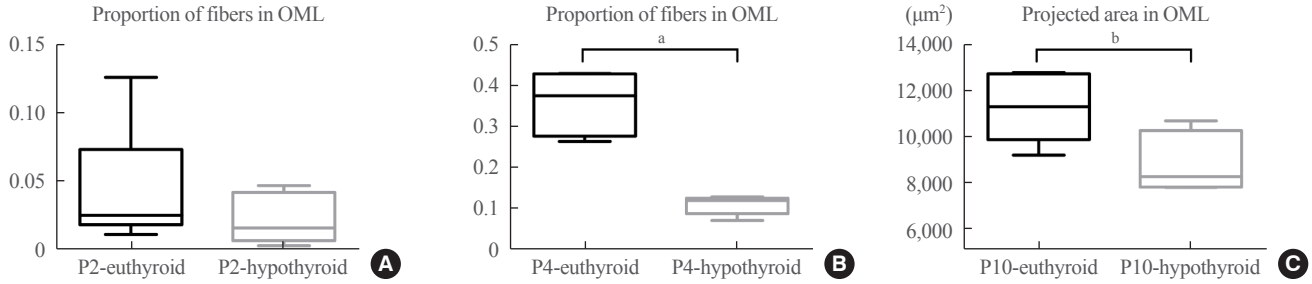

Fig. 4. The proportion of DiI-labeled fibers in the outer molecular layer (OML) at (A) P2, (B) P4, and (C) the projected area in the OML at P10. Slices (n=5–7) from different pups (n=5–7 pups from 5–7 dams) in each group. [a]P<0.001; [b]P=0.027, compared with the euthyroid group.

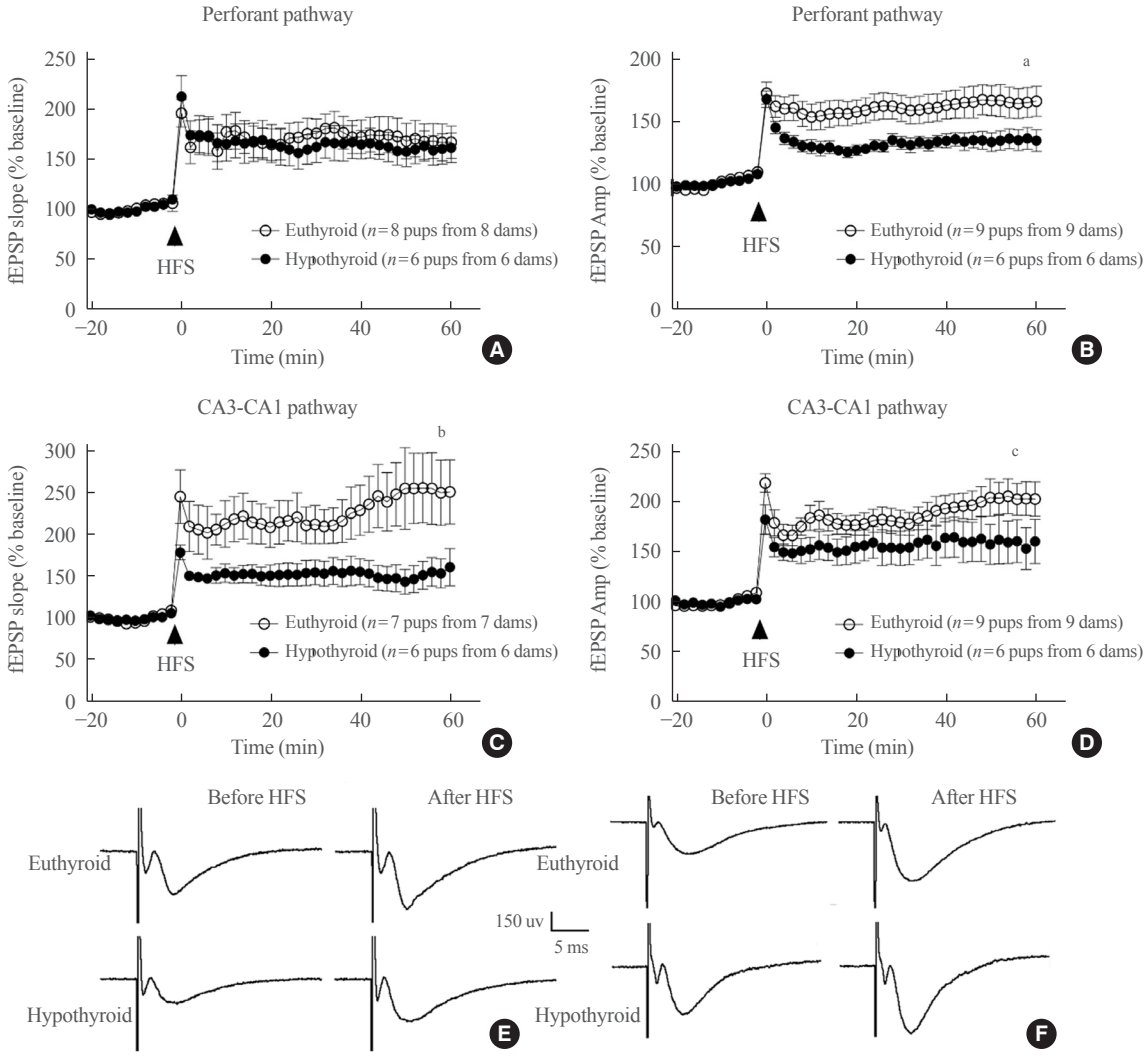

Fig. 5. Long-term potentiation in the perforant pathway and CA3-CA1 pathway assessed as the percent change in the field excitatory postsynaptic potential (fEPSP) slope and fEPSP amplitude (Amp) from baseline at P10. (A, B) For the perforant pathway, there was no significant difference in the fEPSP slope; however, the fEPSP Amp of the hypothyroid pups was lower than that of the euthyroid pups. Slices (n=6–9) were from different pups (n=6–9 pups from 6–9 dams) at P10. (C, D) For the CA3-CA1 pathway, maternal hypothyroidism reduced both the fEPSP slope and the Amp in the pups. Slices (n=6–7) were from different pups (n=6–7 pups from 6–7 dams) at P10. (E, F) Inset: representative waveforms recorded in the perforant and CA3-CA1 pathways before high-frequency stimulation (HFS) and after HFS in the euthyroid and hypothyroid groups. CA, cornu ammonis. [a]P=0.036; [b]P=0.038; [c]P=0.008, compared with the euthyroid group.

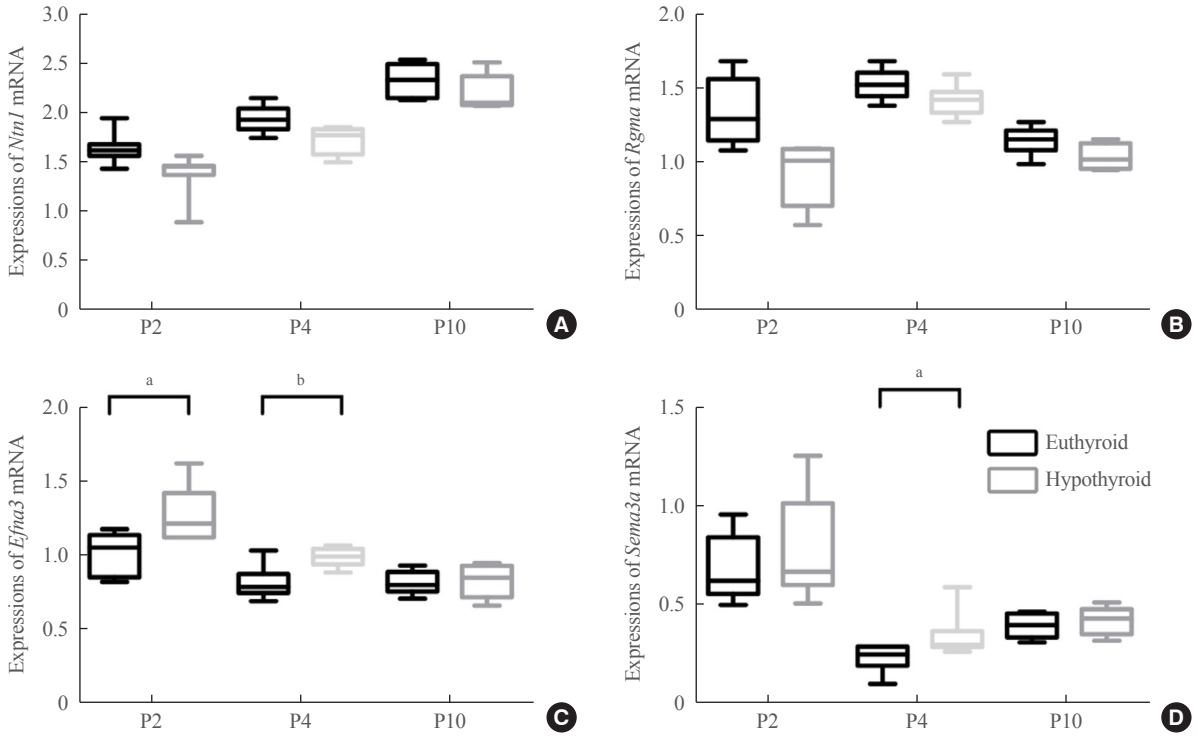

Fig. 6. Expression of (A) netrin 1 (*Ntn1*), (B) repulsive guidance molecule BMP co-receptor A (*Rgma*), (C) erythropoietin-producing hepatocyte ligand A3 (*Efna3*), and (D) semaphorin 3A (*Sema3a*) mRNA in the hippocampus of the euthyroid and hypothyroid groups (n=6–8 pups from 5–6 dams in each group). [a]P<0.05; [b]P<0.01, compared with the euthyroid group.

pothyroid group, P=0.038; fEPSP amplitude: 187.03%±29.41% of baseline in the euthyroid group, 141.30%±19.73% of baseline in the hypothyroid group, P=0.008) (Fig. 5C, D).

Developmental hypothyroidism increased the expression of repulsive axon guidance molecules

We next studied the possible axon guidance molecules that cause delayed development of the entorhinal-dentate gyrus pathway. The attractive (netrin 1) or repulsive (ephrin A3, Sema3a, and Rgma) axon guidance molecules are involved in the formation of the entorhinal-dentate gyrus pathway and act as regulatory signals of entorhinal axons. Our results showed that the mRNA expression levels of *Ntn1* and *Rgma* did not show statistically significant differences between the two groups (Fig. 6A, B).

Real-time PCR showed upregulation of *Efna3* mRNA expression at P2 and P4 in the hypothyroid group (P2: P=0.012; P4: P=0.007) (Fig. 6C). Western blotting showed that the level of ephrin A3 protein was markedly higher in the hypothyroid group than in the euthyroid group at P2 and P4 (P2: P=0.029; P4: P=0.006) (Fig. 7A, B). There was no difference in the expression levels of ephrin A3 mRNA and protein between the two groups at P10.

The expression level of *Sema3a* mRNA increased slightly in the hypothyroid group at P2, but there was no statistically significant difference compared with that in the euthyroid group (Fig. 6D). *Sema3a* mRNA expression was upregulated in the hypothyroid group compared with that in the euthyroid group only at P4 (P=0.046) (Fig. 6D). Western blotting displayed an enhancing effect of maternal hypothyroidism on Sema3a protein levels at P2 and P4 (P2: P=0.005; P4: P=0.012), but not at P10 (Fig. 7A, C).

DISCUSSION

The entorhinal-dentate gyrus pathway starts to develop as early as E16 [31]. To study the role of thyroid hormones in the entorhinal-dentate gyrus pathway development, it is necessary to inhibit the maternal transport and fetal synthesis of thyroid hormones at the early embryonic stage. The model of experimental hypothyroidism in our study was induced by a thyrotoxicant (MMI). Although significant changes in body weight were observed in the pups, MMI did not alter the body weight of the dams during the gestational and lactation periods. Berbel et al.

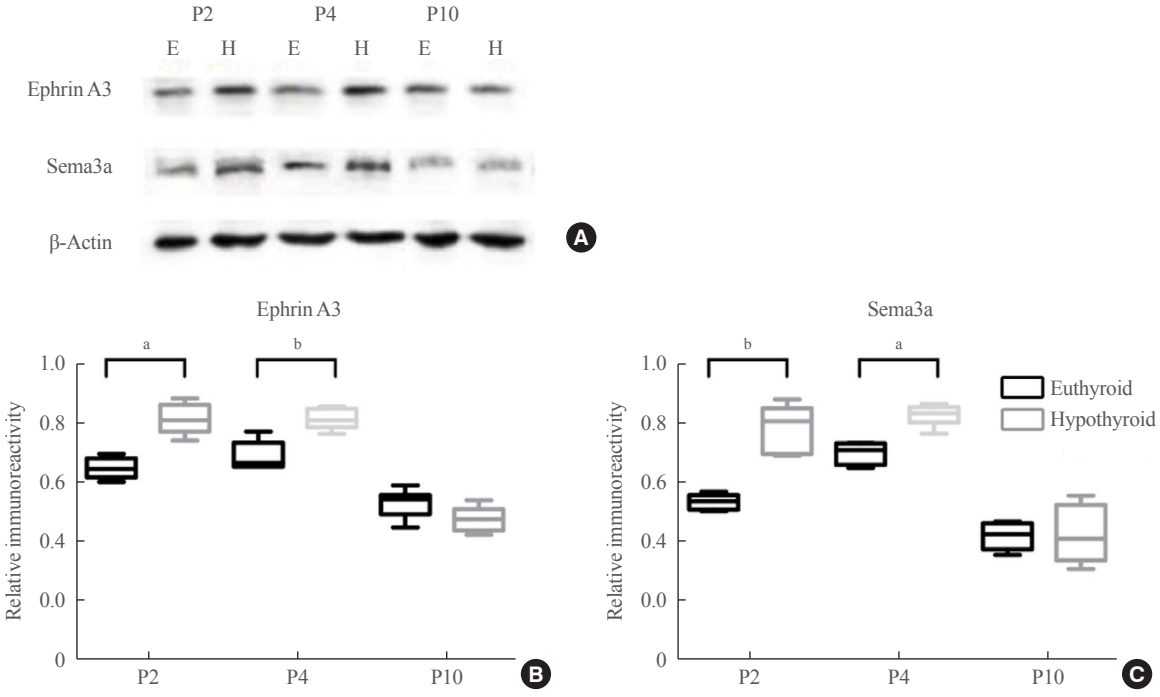

Fig. 7. (A, B, C) Western blotting analysis of ephrin A3 and Sema3a proteins in the hippocampus of the euthyroid and hypothyroid groups ($n=6$ pups from 4–6 dams in each group). The bands (A) depicted representative findings for the euthyroid and hypothyroid groups. The bar graphs (B, C) showed the results of semiquantitative measurements of ephrin A3 and Sema3a. E, euthyroid; H, hypothyroid. [a]$P<0.05$; [b]$P<0.01$, compared with the euthyroid group.

[32] observed that all MMI-treated pregnant rats gave birth at term and the litter size was similar to that of the control rats.

A hypothyroid state could promote a series of hippocampal neuronal functional defects. The hippocampus is considered to be involved in neuronal networks that determine mnemonic, cognitive, and emotional functions. To construct and maintain the mnemonic network, intact fiber circuits are indispensable. The classic fiber circuit of the hippocampus from the entorhinal cortex to the dentate gyrus, to CA3, and then to CA1 contributes to the formation and retrieval of memories [19]. Physical lesions of the entorhinal cortex inputs to the hippocampus were found to lead to impaired episodic-memory processing, such as pattern completion and separation [18,22,33].

The present study is the first study designed to examine the entorhinal-dentate gyrus pathway in the pups of a rat model of developmental hypothyroidism. Axon tracing provided visualization of the entorhinal-dentate gyrus pathway. DiI is the most frequently used carbocyanine dye, which emits red fluorescence. Since DiI is suitable for post-mortem neuronal tracing in fixed tissue, it is particularly useful for studying embryonic pathways [34]. DiI produces labeling by diffusing through the lipid membrane, and has performed well in many aspects in comparative studies. This dye has several potential advantages, including its slow fading, tracing length, nontoxicity, ease of use, and price [35,36]. However, DiI labels the pathway more slowly in fixed tissue than in living tissue and diffuses before reaching the axon terminal in long-distance labeling. Referring to Deng's research on the entorhinal-dentate gyrus pathway, we found that an incubation time of 2 to 3 weeks was suitable because of the low rate of diffusion [31]. Our data indicated that the entorhinal-dentate gyrus pathway experienced delayed development in reaching its destination in the hypothyroid group. In addition, the projected area of entorhinal axons that arrived at the outer molecular layer was significantly smaller in the hypothyroid group than in the euthyroid group. It is possible that the difference in the projected area was affected by confounding factors, such as body weight, the volume of the dentate gyrus, and the ratio of the dentate gyrus volume to the brain volume under a state of hypothyroidism. However, our sample size was not adequate to determine these potential confounders. Berbel et al. [32] (1993) confirmed that the callosally projecting neurons of the auditory areas shifted to the infragranular layers in hypothyroid rats. Subsequently, researchers examined the effects of thyroid hormones on the development of somatosensory thala-

mocortical projections [37]. Anterograde tracing in hypothyroid offspring showed that although the thalamocortical axons reached their normal target, the numbers of terminal branches were reduced. These data underscore the relationship between altered neuronal circuits and the neurological diseases induced by developmental hypothyroidism.

At P10, the formation and distribution of the entorhinal-dentate gyrus pathway were similar between the hypothyroid and euthyroid groups. However, activity-dependent synaptic plasticity (LTP) was impaired. LTP is an established biological substrate for learning and memory, and a series of experiments showed the correlation between decreased LTP and impaired memory function [38]. As described previously, hypothyroidism impaired the LTP of pathways in the hippocampus. For the perforant pathway, the LTP slope was impaired in adult offspring following propylthiouracil treatment of rats [11,15]. However, augmentation of the LTP amplitude was observed, which could have been caused by structural changes in spine morphology in the neurons in hypothyroid animals and might reflect a compensation for reduced synaptic input [39]. This could explain the differential effects on the LTP slope and amplitude in our study. For the CA3-CA1 pathway, congenital iodine deficiency and hypothyroidism caused a reduced LTP slope and amplitude [40]. Maternal subclinical hypothyroidism and clinical hypothyroidism both led to LTP slope reduction in pups [14]. However, previously used experimental animals were almost all adult offspring. In the present study, we chose P10 to investigate synaptic transmission and plasticity, including the perforant and CA3-CA1 pathways. The synaptic function of the hippocampus exhibits developmental progression during the postnatal period. Intracellular recordings of previous studies revealed that the dentate gyrus and CA1 regions exhibited LTP at early P7-8 [41-43]. Our data showed that developmental hypothyroidism resulted in LTP impairment, including the slope and amplitude, which is consistent with impaired development of the entorhinal-dentate gyrus pathway.

Many diffusible and membrane-associated attractive or repulsive axon guidance molecules are involved in the neuroanatomical formation of the entorhinal-dentate gyrus pathway. These molecules include netrin, semaphorins, Rgma, and ephrin tyrosine kinase receptors and their ligands [44,45]. In the developing hippocampus, the site-specific expression of molecules at the appropriate time suggests their roles in shaping the entorhinal-dentate gyrus pathway. It has been shown that ephrin A3 and Sema3a are localized in the granule cell layer of the dentate gyrus, where entorhinal axons could not invade [46,47]. The entorhinal axons could be specifically repelled by the two molecules to allow the entorhinal-dentate gyrus pathway to enter the target area in the molecular layer of the dentate gyrus. In the present study, the levels of ephrin A3 and Sema3a were upregulated in the hypothyroid group before the afferents reached the outer molecular layer of the dentate gyrus. Although speculative, this would partially explain the impaired development of the entorhinal-dentate gyrus pathway. However, the mechanism by which developmental hypothyroidism upregulated the expression levels of the *Efna3* and *Sema3a* genes is unclear. Meanwhile, there were no significant changes in the levels of those two molecules at P10 between the euthyroid and hypothyroid groups. We hypothesize that this could be caused by the redundancy of these axon guidance molecules when the entorhinal-dentate gyrus pathway is formed. In addition to axon guidance molecules, other mechanisms could contribute to the impaired development of the entorhinal-dentate gyrus pathway resulting from hypothyroidism. Thyroid hormones are required for neuron differentiation and synaptogenesis; for example, the pyramidal cells of the neocortex and hippocampus, and the Purkinje cells of the cerebellum [48]. The stellate cells of the entorhinal cortex, which send projections to the dentate gyrus, are possibly influenced by thyroid hormone deficiency. Another related mechanism is via Cajal-Retzius cells. Reelin, which is produced by Cajal-Retzius cells, is essential to establish the neocortical layers and is under thyroid hormone control [49]. Moreover, Cajal-Retzius cells in the hippocampus are pioneer neurons that guide the perforant pathway [50,51].

Our study had some limitations. Although we found that developmental hypothyroidism resulted in impaired structural development and synaptic plasticity of the entorhinal-dentate gyrus pathway, we did not further investigate dendritic growth, dendritic morphology, and synaptic formation. Another limitation was that we did not assess myelination impairment resulting from thyroid hormone deficiency, which might have influenced the DiI tracing. Finally, we did not design another group with developmental hypothyroidism and added thyroid hormone. This treatment group would have provided more data to determine the reverse effects of thyroid hormone.

We reported that developmental hypothyroidism resulted in impaired development of the entorhinal-dentate gyrus pathway of the offspring, which could contribute to the impaired LTP. Our findings offer potential insights into the functional defects of fiber pathway development, which might be a direction for future study.

CONFLICTS OF INTEREST

No potential conflict of interest relevant to this article was reported.

ACKNOWLEDGMENTS

This study was funded by the Chinese National Natural Science Foundation Grants 81970681 and 81570711 to Xiaochun Teng. We thank Professor Jinbo Deng (Henan University) for technical support in the DiI Tract Tracing.

AUTHOR CONTRIBUTIONS

Conception or design: T.J., W.T., X.T. Acquisition, analysis, or interpretation of data: T.J., R.W., S.P., X.L., H.Z., X.H. Drafting the work or revising: T.J., X.T. Final approval of the manuscript: T.J., X.T.

ORCID

Ting Jin *https://orcid.org/0000-0002-8688-0445*
Ranran Wang *https://orcid.org/0000-0002-8585-7905*
Xiaochun Teng *https://orcid.org/0000-0003-1329-8486*

REFERENCES

1. Wang W, Teng W, Shan Z, Wang S, Li J, Zhu L, et al. The prevalence of thyroid disorders during early pregnancy in China: the benefits of universal screening in the first trimester of pregnancy. Eur J Endocrinol 2011;164:263-8.
2. LaFranchi SH, Haddow JE, Hollowell JG. Is thyroid inadequacy during gestation a risk factor for adverse pregnancy and developmental outcomes? Thyroid 2005;15:60-71.
3. Ahmed OM, El-Gareib AW, El-Bakry AM, Abd El-Tawab SM, Ahmed RG. Thyroid hormones states and brain development interactions. Int J Dev Neurosci 2008;26:147-209.
4. Bernal J, Guadano-Ferraz A, Morte B. Perspectives in the study of thyroid hormone action on brain development and function. Thyroid 2003;13:1005-12.
5. Giese KP, Fedorov NB, Filipkowski RK, Silva AJ. Autophosphorylation at Thr286 of the alpha calcium-calmodulin kinase II in LTP and learning. Science 1998;279:870-3.
6. Rogan MT, Staubli UV, LeDoux JE. Fear conditioning induces associative long-term potentiation in the amygdala. Nature 1997;390:604-7.
7. Whitlock JR, Heynen AJ, Shuler MG, Bear MF. Learning induces long-term potentiation in the hippocampus. Science 2006;313:1093-7.
8. Miller S, Mayford M. Cellular and molecular mechanisms of memory: the LTP connection. Curr Opin Genet Dev 1999;9:333-7.
9. Lynch MA. Long-term potentiation and memory. Physiol Rev 2004;84:87-136.
10. Nicoll RA. A brief history of long-term potentiation. Neuron 2017;93:281-90.
11. Gilbert ME, Sui L. Dose-dependent reductions in spatial learning and synaptic function in the dentate gyrus of adult rats following developmental thyroid hormone insufficiency. Brain Res 2006;1069:10-22.
12. Opazo MC, Gianini A, Pancetti F, Azkcona G, Alarcon L, Lizana R, et al. Maternal hypothyroxinemia impairs spatial learning and synaptic nature and function in the offspring. Endocrinology 2008;149:5097-106.
13. Alzoubi KH, Gerges NZ, Aleisa AM, Alkadhi KA. Levothyroxin restores hypothyroidism-induced impairment of hippocampus-dependent learning and memory: behavioral, electrophysiological, and molecular studies. Hippocampus 2009;19:66-78.
14. Zhang Y, Fan Y, Yu X, Wang X, Bao S, Li J, et al. Maternal subclinical hypothyroidism impairs neurodevelopment in rat offspring by inhibiting the CREB signaling pathway. Mol Neurobiol 2015;52:432-41.
15. Gilbert ME, Paczkowski C. Propylthiouracil (PTU)-induced hypothyroidism in the developing rat impairs synaptic transmission and plasticity in the dentate gyrus of the adult hippocampus. Brain Res Dev Brain Res 2003;145:19-29.
16. McClelland JL, McNaughton BL, O'Reilly RC. Why there are complementary learning systems in the hippocampus and neocortex: insights from the successes and failures of connectionist models of learning and memory. Psychol Rev 1995;102:419-57.
17. Steffenach HA, Witter M, Moser MB, Moser EI. Spatial memory in the rat requires the dorsolateral band of the entorhinal cortex. Neuron 2005;45:301-13.
18. Basu J, Siegelbaum SA. The corticohippocampal circuit, synaptic plasticity, and memory. Cold Spring Harb Perspect Biol 2015;7:a021733.
19. Witter MP. The perforant path: projections from the entorhinal cortex to the dentate gyrus. Prog Brain Res 2007;163:43-61.
20. Ahmed OJ, Mehta MR. The hippocampal rate code: anatomy, physiology and theory. Trends Neurosci 2009;32:329-

38.
21. Bartesaghi R, Gessi T, Migliore M. Input-output relations in the entorhinal-hippocampal-entorhinal loop: entorhinal cortex and dentate gyrus. Hippocampus 1995;5:440-51.
22. Kesner RP, Gilbert PE, Wallenstein GV. Testing neural network models of memory with behavioral experiments. Curr Opin Neurobiol 2000;10:260-5.
23. Bernal J. Thyroid hormones and brain development. Vitam Horm 2005;71:95-122.
24. Koromilas C, Liapi C, Schulpis KH, Kalafatakis K, Zarros A, Tsakiris S. Structural and functional alterations in the hippocampus due to hypothyroidism. Metab Brain Dis 2010;25:339-54.
25. Auso E, Lavado-Autric R, Cuevas E, Del Rey FE, Morreale De Escobar G, et al. A moderate and transient deficiency of maternal thyroid function at the beginning of fetal neocorticogenesis alters neuronal migration. Endocrinology 2004;145:4037-47.
26. Wong CC, Leung MS. Effects of neonatal hypothyroidism on the expressions of growth cone proteins and axon guidance molecules related genes in the hippocampus. Mol Cell Endocrinol 2001;184:143-50.
27. Alvarez-Dolado M, Figueroa A, Kozlov S, Sonderegger P, Furley AJ, Munoz A. Thyroid hormone regulates TAG-1 expression in the developing rat brain. Eur J Neurosci 2001;14:1209-18.
28. Tamamaki N. Organization of the entorhinal projection to the rat dentate gyrus revealed by Dil anterograde labeling. Exp Brain Res 1997;116:250-8.
29. He Y, Liu MG, Gong KR, Chen J. Differential effects of long and short train theta burst stimulation on LTP induction in rat anterior cingulate cortex slices: multi-electrode array recordings. Neurosci Bull 2009;25:309-18.
30. Miao HH, Li XH, Chen QY, Zhuo M. Calcium-stimulated adenylyl cyclase subtype 1 is required for presynaptic long-term potentiation in the insular cortex of adult mice. Mol Pain 2019;15:1744806919842961.
31. Deng JB, Yu DM, Wu P, Li MS. The tracing study of developing entorhino-hippocampal pathway. Int J Dev Neurosci 2007;25:251-8.
32. Berbel P, Guadano-Ferraz A, Martinez M, Quiles JA, Balboa R, Innocenti GM. Organization of auditory callosal connections in hypothyroid adult rats. Eur J Neurosci 1993;5:1465-78.
33. Kitamura T. Driving and regulating temporal association learning coordinated by entorhinal-hippocampal network. Neurosci Res 2017;121:1-6.
34. Godement P, Vanselow J, Thanos S, Bonhoeffer F. A study in developing visual systems with a new method of staining neurones and their processes in fixed tissue. Development 1987;101:697-713.
35. Heilingoetter CL, Jensen MB. Histological methods for ex vivo axon tracing: a systematic review. Neurol Res 2016;38:561-9.
36. Chen BK, Miller SM, Mantilla CB, Gross L, Yaszemski MJ, Windebank AJ. Optimizing conditions and avoiding pitfalls for prolonged axonal tracing with carbocyanine dyes in fixed rat spinal cords. J Neurosci Methods 2006;154:256-63.
37. Auso E, Cases O, Fouquet C, Camacho M, Garcia-Velasco JV, Gaspar P, et al. Protracted expression of serotonin transporter and altered thalamocortical projections in the barrelfield of hypothyroid rats. Eur J Neurosci 2001;14:1968-80.
38. Silva AJ. Molecular and cellular cognitive studies of the role of synaptic plasticity in memory. J Neurobiol 2003;54:224-37.
39. Madeira MD, Paula-Barbosa MM. Reorganization of mossy fiber synapses in male and female hypothyroid rats: a stereological study. J Comp Neurol 1993;337:334-52.
40. Dong J, Yin H, Liu W, Wang P, Jiang Y, Chen J. Congenital iodine deficiency and hypothyroidism impair LTP and decrease C-fos and C-jun expression in rat hippocampus. Neurotoxicology 2005;26:417-26.
41. Duffy CJ, Teyler TJ. Development of potentiation in the dentate gyrus of rat: physiology and anatomy. Brain Res Bull 1978;3:425-30.
42. Hussain RJ, Carpenter DO. Development of synaptic responses and plasticity at the SC-CA1 and MF-CA3 synapses in rat hippocampus. Cell Mol Neurobiol 2001;21:357-68.
43. Yasuda H, Barth AL, Stellwagen D, Malenka RC. A developmental switch in the signaling cascades for LTP induction. Nat Neurosci 2003;6:15-6.
44. Skutella T, Nitsch R. New molecules for hippocampal development. Trends Neurosci 2001;24:107-13.
45. Brinks H, Conrad S, Vogt J, Oldekamp J, Sierra A, Deitinghoff L, et al. The repulsive guidance molecule RGMa is involved in the formation of afferent connections in the dentate gyrus. J Neurosci 2004;24:3862-9.
46. Chedotal A, Del Rio JA, Ruiz M, He Z, Borrell V, de Castro F, et al. Semaphorins III and IV repel hippocampal axons via two distinct receptors. Development 1998;125:4313-23.
47. Stein E, Savaskan NE, Ninnemann O, Nitsch R, Zhou R, Skutella T. A role for the Eph ligand ephrin-A3 in entorhino-

hippocampal axon targeting. J Neurosci 1999;19:8885-93.
48. Santisteban P, Bernal J. Thyroid development and effect on the nervous system. Rev Endocr Metab Disord 2005;6:217-28.
49. Bernal J. Action of thyroid hormone in brain. J Endocrinol Invest 2002;25:268-88.
50. Ceranik K, Zhao S, Frotscher M. Development of the entorhino-hippocampal projection: guidance by Cajal-Retzius cell axons. Ann N Y Acad Sci 2000;911:43-54.
51. Zhao S, Chai X, Forster E, Frotscher M. Reelin is a positional signal for the lamination of dentate granule cells. Development 2004;131:5117-25.